The Sensitivity of Millimeter and Sub-millimeter Frequencies to Atmospheric Temperature and Water Vapor Variations

Marian KLEIN and Albin J. GASIEWSKI
NOAA Environmental Technology Laboratory
R/E/ET1, 325 Broadway, Boulder, Colorado, USA 80303
Telephone: (303) 497-6418, (303) 497-7275, Fax: (303) 497-3577, E-mail: mklein@etl.noaa.gov, agasiewski@etl.noaa.gov

Abstract - In order to determine optimal sounding strategies for future high resolution passive microwave instruments from space a study of the potential sounding capabilities of all significant microwave oxygen and water vapor absorption lines in the frequency range from approximately 10 to 1000 GHz has been undertaken. The study uses a second-order statistical climatological model covering four seasons and three latitudinal zones: low (30°S to 30°N), middle (30° to 60°) and high (60° to 90°) latitudes, and a wide range of altitudes (up to ~70 km). The climatological model was developed using data from three sources: the UARS HALOE instrument, the TOVS Initial Guess Retrieval (TIGR) radiosonde set and the NOAA AMSU radiosonde set. Variations in the vertical sensitivities of brightness temperature due to statistical variations of water vapor and temperature with latitude and season around each line are considered and useful channel sets for geostationary microwave vertical sounding are suggested.

INTRODUCTION

Historically, microwave frequencies that have been used for water vapor sounding are those around the 22.2351 and 183.3101 GHz water vapor absorption lines, e.g. the SSM/I and SSM/T-2, and AMSU instruments. Frequencies used for passive microwave temperature sounding are those located between 50-60 GHz, e.g. MSU, AMSU, SSM/T-1. To obtain the dwell time and sampling rate necessary for the observation of severe weather conditions it is desirable to place microwave imagers/sounders on geostationary platforms, for example the proposed NOAA GOES Geosynchronous Microwave Sounder [1]. However, the geosynchronous distance requires that higher microwave frequencies than those currently used be used to provide good resolution (<20 km spot size) using diffraction limited apertures of reasonable size (~2-3 m). The objective of this study is to assess the utility of all significant absorption lines within the frequency range of ~10-1000 GHz for passive microwave sounding of water vapor and temperature from satellites.

INCREMENTAL WEIGHTING FUNCTIONS

The incremental weighting functions (IWF) describe the relationship between infinitesimal variations in any atmospheric parameter and the upwelling (or downwelling) brightness temperature. If $\delta p(z)$ is the variation in the profile of the atmospheric parameter of concern, then the variation in upwelling brightness is obtained by:

$$\delta T_B(f,\theta) = \int \delta p(z) W(z,f,\theta) dz \qquad (1)$$

where W_p is the incremental weighting function for parameter p, and θ is the observation angle measured with respect to nadir. The parameters of concern for this study are temperature and water vapor density. The IWF provides information about the vertical sensitivity to the observed parameter, thus it is a useful tool for sensitivity studies, inversion, and assimilation.

The water vapor IWF derived from the nonscattering solution to the radiative transfer equation for a downward looking radiometer is:

$$W_\rho^{\uparrow}(f,z,\theta) = \left.\frac{\partial \alpha(f,T(z),\rho(z))}{\partial \rho}\right|_{\rho^0(z)} \sec\theta e^{-\tau(f,z,h)\sec\theta} \left\{ T_B(f,T(z)) - T_B^{0\downarrow RE} e^{-\tau(f,0,z)\sec\theta} - \int_0^z T_B(f,T(z'))\alpha(f,T(z'),\rho(z'))\sec\theta e^{-\tau(f,z',z)\sec\theta} dz' \right\} + W_\rho^{\downarrow R}(f,z,\theta) \qquad (2)$$

in units, e.g. $(K\,km^{-1}\,g^{-1}\,m^3)$, where:

$$W_\rho^{\downarrow R}(f,z,\theta) = e^{-\tau(f,0,h)\sec\theta} r_\beta(\theta) W_\rho^{\downarrow}(f,z,\theta)$$

and $W_\rho^{\downarrow}(f,z,\theta)$ is the water vapor IWF for an upward looking radiometer:

$$W_\rho^{\downarrow}(f,z,\theta) = \left.\frac{\partial \alpha(f,T(z),\rho(z))}{\partial \rho}\right|_{\rho^0(z)} \sec\theta e^{-\tau(f,h,z)\sec\theta} \left\{ T_B(f,T(z)) - T_B(f,T_{CB}) e^{-\tau(f,h,\infty)\sec\theta} - \int_z^\infty T_B(f,T(z'))\alpha(f,T(z'),\rho(z'))\sec\theta e^{-\tau(f,z,z')\sec\theta} dz' \right\}$$

$$T_B^{0\downarrow RE} = (1 - r_\beta(\theta)) T_B(f,T_S) + r_\beta(\theta) T_B(f,0,\infty)$$

$$T_B(f,0,\infty) = \int_0^\infty T_B(f,T(z))\alpha(f,T(z),\rho(z))\sec\theta e^{-\tau(f,0,z)\sec\theta} dz + T_B(f,T_{CB}) e^{-\tau(f,0,\infty)\sec\theta}$$

and $\tau(f,z_1,z_2)$ is the opacity between level z_1 and z_2. The terms in the above equations are: T_B - the equivalent radiation temperature (or brightness temperature) in Kelvins as given

by the Planck law, f - frequency, α - total absorption coefficient, $T(z)$ - physical temperature at atmospheric height z, $\rho(z)$ - water vapor density, h - observation height, r_β - surface reflection coefficient for polarization β, T_S - surface temperature, and T_{CB} - cosmic background temperature. The temperature IWF for a downward looking radiometer can be similarly calculated.

CLIMATOLOGICAL STATISTICS

Atmospheric water vapor statistics vary considerably with season, location, and altitude. Calculations of the water vapor IWF reveal rather enormous sensitivities (of order $\sim 10^6$ $K\,km^{-1}\,g^{-1}\,m^3$) at the center of absorption lines at upper stratospheric and mesospheric altitudes. The total mean amount of water vapor, however, is typically between 2-3 ppmv at these levels, and changes are small enough that it can be expected that the brightness response to water vapor at these altitudes will be moderate. To analyze this response it is necessary to incorporate into the calculation the natural variation of water vapor in the atmosphere. We have thus developed a second order statistical model for temperature and humidity covering altitudes up to ~70 km and a variety of latitudes and seasons.

Three sources of data were used: (1) the HALOE instrument on board the Upper Atmosphere Research Satellite [3], (2) TOVS Initial Guess Retrieval (TIGR) set [4] based on radiosonde and rocketsonde measurements, and (3) the NOAA AMSU radiosonde set. Covariance and correlation matrices were evaluated for all three databases for temperature and water vapor over valid latitude ranges. Overall reasonable agreement in all seasonal/latitudinal bins was found among the three sets. The TIGR database was selected for further studies because of its extensive global coverage and water vapor profile information over the full altitude range.

CONCLUSIONS

The nadir IWFs for temperature and water vapor were evaluated on a non-uniform frequency grid from 10 to 1000 GHz assuming an ocean background [5], an observation height of 150 km, and clear air conditions. The frequency grid density is inversely proportional to the proximity of the closest absorption line, but includes no points closer than 2.5 MHz to any line center. The program used for the calculations is Microwave Radiative Transfer (MRT), version 5.0 [6]. The absorption model is based on Liebe's model [7,8] but does not include Zeeman splitting. The validity of the results is thus restricted up to ~40 km altitude near oxygen absorption lines.

Figs. 1 and 3 show the effective water vapor (p=ρ) and temperature (p=T) sensing heights h_{eff} for two extreme atmospheric cases, along with the IWF widths σ_h, where:

$$h_{eff} = \frac{\int_0^\infty z\left|W_p(f,z,\theta)\right|dz}{\int_0^\infty \left|W_p(f,z,\theta)\right|dz} \tag{4}$$

$$\sigma_h = \sqrt{\frac{\int_0^\infty (z-h_{eff})^2\left|W_p(f,z,\theta)\right|dz}{\int_0^\infty \left|W_p(f,z,\theta)\right|dz}} \tag{5}$$

In equations (4) and (5) water vapor IWFs were multiplied by the standard deviation profile of water vapor for the appropriate seasons and latitudinal zones. Figs. 2 and 4 show the upwelling brightness temperature variations σ_{TB} due to the natural variation of water vapor in the atmosphere:

$$\sigma_{TB} = \sqrt{\overline{W}_p^t \overline{\overline{R}}_{pp} \overline{W}_p} \tag{6}$$

where $\overline{W}_p$ is the incremental (column) weighting vector and $\overline{\overline{R}}_{pp}$ is the covariance matrix for parameter p. The variation σ_{TB} is the minimum sensitivity that the radiometer measuring the parameter of interest must possess in order to be able to sense natural atmospheric variations.

Tables 1 and 2 summarize the calculations for the most significant water vapor and oxygen absorption lines. Since higher frequency channels are generally more attenuated by water vapor it is possible to use them to sound water vapor at higher altitudes. Use of higher frequency channels also allows improved spatial resolution for the same antenna size since spot area decreases with the square of the frequency. Further, the scattering coefficient α_S for spherical Rayleigh ice cloud particles follows f^4a^6 where f is the frequency and a is the particle diameter, see e.g. [2], pp.102. The dramatic increase of α_S with frequency (Tables 1 and 2) illustrates the potential to measure cirrus cloud ice water path. The major disadvantage is the adverse effect of increased cloud opacity on water vapor sounding. However, this disadvantage can be partially offset by using a pair of water vapor sounding bands spaced approximately one to three octaves apart. Other disadvantages of using higher frequency channels are associated with higher water vapor attenuation that obscures the lower levels of the atmosphere. Moreover, the nascent receiver technology at high frequencies results in higher system noise temperatures.

Seasonally and latitudinally varying amounts of water vapor cause significant variation in sounding altitudes. For the two extreme cases the effective height for the same frequency can vary by a factor of nearly two, thus indicating the necessity of nonlinear or geographically indexed water vapor retrieval methods. The standard deviation of brightness temperature σ_{TB} is also influenced by the season, latitude, diurnal period, and location on the globe.

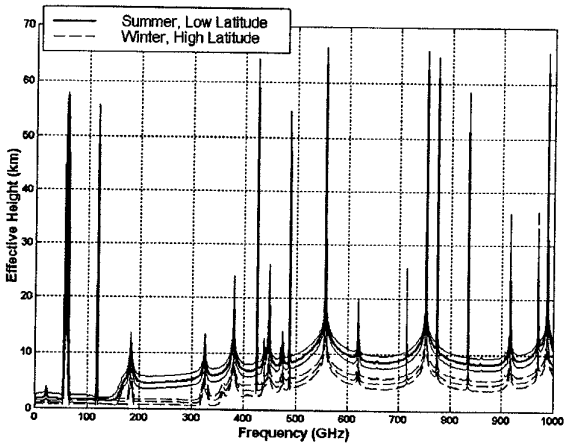

Fig. 1: Effective water vapor sensing height h_{eff} along with $h_{eff} \pm \sigma_h$ for two extreme atmospheric profiles, satellite nadir view over ocean background.

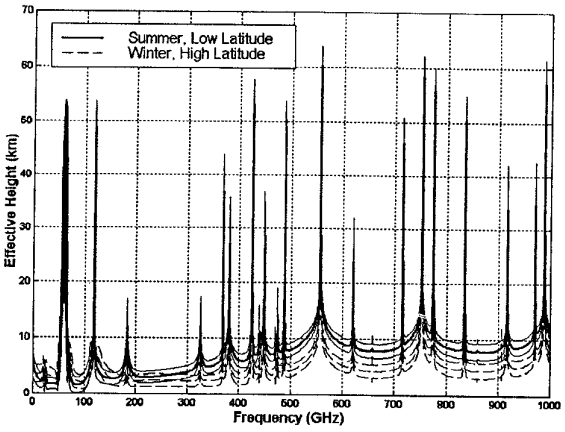

Fig. 3: Effective temperature sensing height h_{eff} along with $h_{eff} \pm \sigma_h$ for two extreme atmospheric profiles, satellite nadir view over ocean background.

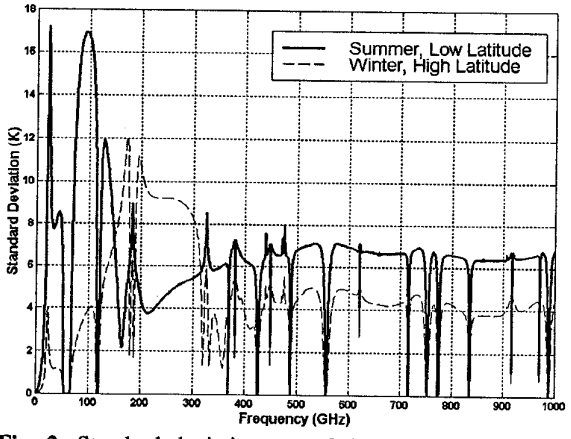

Fig. 2: Standard deviation σ_{TB} of the upwelling brightness temperature due to the water vapor variations for two extreme atmospheric profiles, nadir view over ocean background.

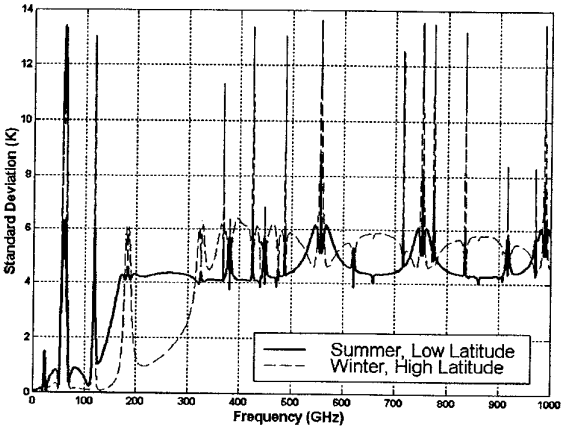

Fig. 4: Standard deviation σ_{TB} of the upwelling brightness temperature due to the temperature variations for two extreme atmospheric profiles, nadir view over ocean background.

Table 1. Vertical sensing capabilities near selected water vapor lines as compared to the 183.3101 GHz absorption line.

Line (GHz)	Approximate Frequency Range (GHz)	Effective Sensing Heights (km) Winter High latitude	Summer Low latitude	σ_{TB} (K)	Relative Spot Area	Relative Rayleigh Scattering Coefficient
183.3101	121 - 183	1.6 - 6.4	2 - 11.8	1.8 - 12	1.00	1.0
325.1529	219 - 325	1.6 - 6.4	5 - 11.6	1.3 – 8.5	0.32	9.9
380.1974	341 - 380	2.2 - 19	6.2 - 20	1.2 – 7.3	0.23	18.5
448.0011	448 - 465	4.4 - 20	8.1 - 21	1.4 – 7.1	0.17	35.7
556.9360	492 – 557	4.9 - 61	8.6 - 64	0.04 – 7.1	0.11	85.2
752.0332	717 – 752	5.8 - 60	9.8 - 63	0.06 – 7.0	0.06	283.3
987.9268	975 - 988	7.4 - 60	11.9 - 63	0.07 – 6.8	0.03	843.6

Table 2. Vertical sensing capabilities near selected oxygen absorption lines as compared to the oxygen absorption lines within the frequency band 50-70 GHz. The symbol "S" implies the surface height.

Line (GHz)	Approximate Frequency Range (GHz)	Effective Sensing Heights (km) Winter High latitude	Summer Low latitude	σ_{TB} (K)	Relative Spot Area	Relative Rayleigh Scattering Coefficient
50-70	43 - 86	S – 40+	S - 40+	0.3 - 10.6	1	1
118.7503	86 - 119	S - 40+	S - 40+	0.15 - 10.2	0.255	15.3
368.4984	341 - 369	S - 35.4	4.9 - 36.8	4.1 - 7.0	0.027	1.4×10^3
424.7631	402 - 425	S - 40+	6.1 - 40+	1.2 - 11.2	0.020	2.5×10^3
487.2494	481 - 487	4.0 - 40+	7.6 - 40+	4.3 - 10.2	0.015	4.3×10^3
715.3932	668 - 715	4.3 - 40+	7.9 - 40+	4.3 - 9.3	0.007	2.0×10^4
773.8387	719 - 774	5.6 - 40+	9.3 - 40+	4.71 - 11.5	0.006	2.8×10^4
834.1453	824 - 834	4.7 - 40+	8.2 - 40+	4.4 - 10.6	0.005	3.7×10^4

Table 1 is a comparison of the sounding capabilities of the 183.3101 GHz water vapor absorption line with major lines at higher frequencies. The observable sounding altitudes extend from the surface to the upper stratosphere. Although Fig. 1 and Table 1 imply the possibility of sounding in the lower mesosphere, the narrow bandwidth required and low σ_{TB} may preclude adequate sensitivity. For example, assuming a total power radiometer with 10,000 K system temperature, 300 MHz bandwidth, and 10 seconds integration time, ΔT_{RMS} is ~0.2 K, and it is possible to sense water vapor variations in the vicinity of the 556.9360 GHz line up to an altitude of ~40 km.

Fig. 3 and Table 2 shows less seasonal and latitudinal variation in the effective sounding altitude for the temperature than for water vapor. For geostationary purposes a combination of the 118.7503 GHz and 424.7631 GHz lines provide vertical coverage nearly comparable to that of the 50-70 GHz band.

For geosynchronous sounding it is suggested that a suite of several channels around the following window and line frequencies would provide good vertical coverage from the surface to the lower stratosphere:

(a) 118.7503/150/166/183.3101 GHz (for cloud penetrability, temperature and water vapor profiling, and water vapor observational heritage).

(b) 220/325.1529 or 340/380.1974 GHz (for cloud detection and high spatial resolution. Here, 380.1974 GHz would provide unique upper troposphere/lower stratosphere water vapor sensitivity).

(c) 402/424.7631 GHz (for temperature profiling and high resolution raincell mapping).

Higher frequencies than the above could provide even better cloud detectability and higher altitude water vapor sounding, but would require improvements in receiver technology.

References

[1] Staelin, D. H., Kerekes, J. P., Solman, F. J. III.: "Geosynchronous microwave sounder working group, Final report", Massachusetts Institute of Technology, Lincoln Laboratory, Lexington, Massachusetts, August 22, 1997.

[2] Gasiewski, A. J.: "Microwave radiative transfer in hydrometeors," in "Atmospheric remote sensing by microwave radiometry" edited by Janssen, M. A., Wiley & sons, New York, 1993, ch.3.

[3] Russel, J.M. III, L. L. Gordley, J. H. Park, S. R. Drayson, W. D. Hesketh, R. J. Cicerone, A. F. Tuck, J. E. Frederick, J. E. Harries, P. J. Crutzen: "The halogen occultation experiment", Journal of Geophysical Research, Vol. 98, No. D6, pp.10 777-10 797, June20, 1993.

[4] Chedin, A., Scott, N. A., Wahiche, C., and Mouliner, P.: "The improved initialization inversion method: A high resolution physical method for temperature retrievals from satellites of the TIROS-N series", Journal of Climate and Applied Meteorology, Vol. 24, pp. 128-143, February 1985.

[5] Wilheit, T. T., Jr.: "A model for the microwave emissivity of the ocean's surface as a function of wind speed", IEEE Transaction on Geoscience Electronics, Vol. GE-17, No. 4, pp. 244-249, October 1979.

[6] Gasiewski, A. J. and Staelin, D. H.: "Numerical modeling of passive microwave O_2 observations over precipitation", Radio Science, Vol. 25, No. 3, pp. 217-235, May-June 1990.

[7] Liebe, H. J.: "An atmospheric millimeter wave propagation model", NTIA Report 83-137, US Department of Commerce, December 1983.

[8] Liebe, H. J.: "A contribution to modeling atmospheric millimeter-wave properties", Frequenz, Vol. 41, No. 1-2, pp. 31-36, January-February 1987.